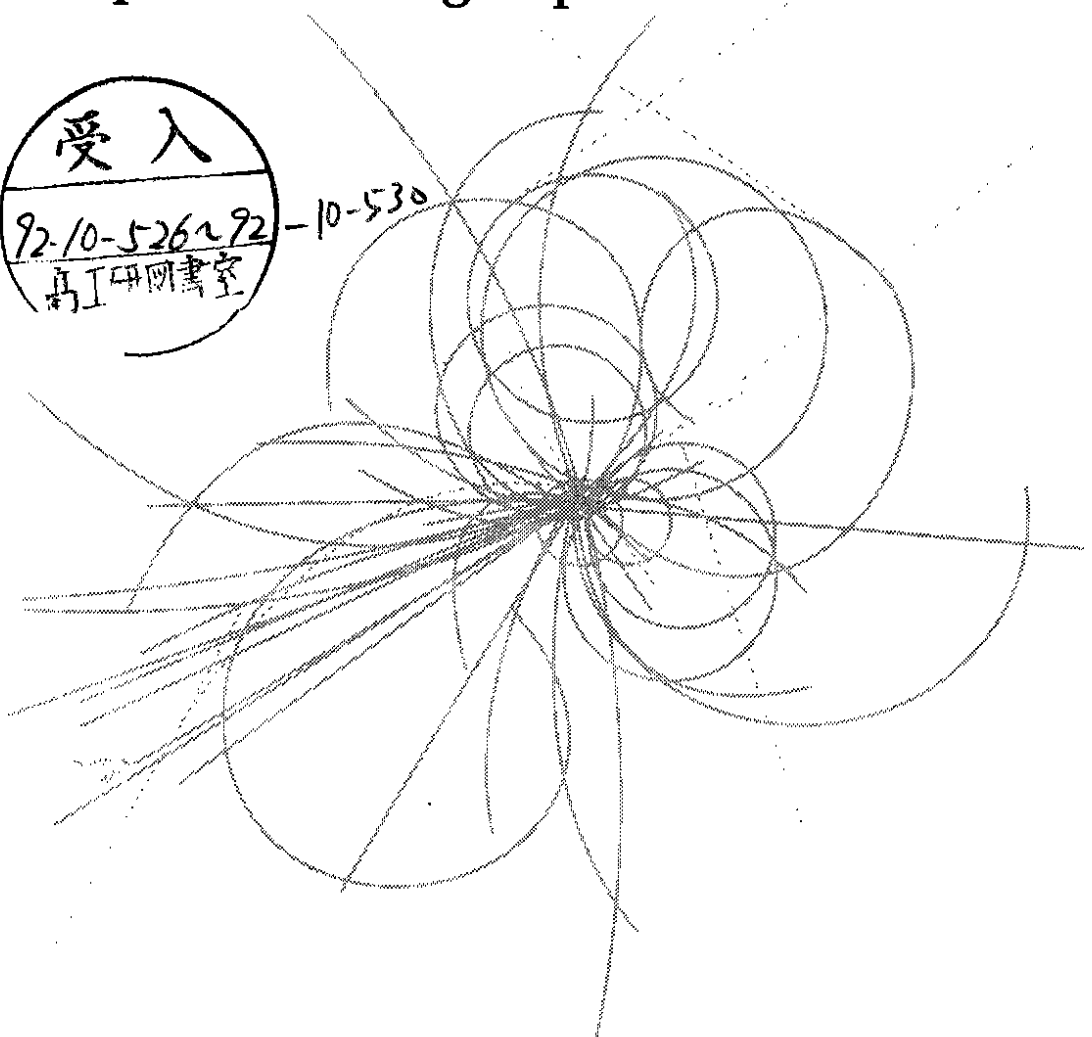


Superconducting Super Collider Laboratory



Papers Contributed to the 1992 Applied Superconductivity Conference

The Magnet Test Analysis Group

August 1992

**Papers Contributed to the 1992 Applied
Superconductivity Conference**

The Magnet Test Analysis Group

Accelerator Design and Operations Division
Superconducting Super Collider Laboratory[†]
2550 Beckleymeade Ave.
Dallas, TX 75237

August 1991

[†]Operated by the Universities Research Association, Inc., for the U.S. Department of Energy under Contract No. DE-AC35-89ER40486.

Mechanical Performance of 5-cm-Aperture, 15-m-Long SSC Dipole Magnet Prototypes*

T. Ogitsu,^{1,4} A. Akhmetov,¹ M. Anerella,² R. Bossert,³ T. Bush,¹ D.W. Capone II,¹ J. Carson,³ R. Coombes,¹ J. Cottingham,² S.W. Delchamps,³ A. Devred,¹ J. DiMarco,¹ G. Ganetis,² M. Garber,² C. Goodzeit,¹ A. Ghosh,² S. Gourlay,³ A. Greene,² R. Gupta,² R. Hanft,³ A. Jain,² S. Kahn,² E. Kelly,² W. Koska,³ M. Kuchnir,³ J. Kuzminski,¹ M.J. Lamm,³ P. Mantsch,³ P.O. Mazur,³ G. Morgan,² J. Muratore,² W. Nah,^{1,5} D. Orris,³ J. Ozelis,³ T. Peterson,³ E.G. Pewitt,³ A. Prodell,² M. Puglisi,¹ P. Radusewicz,¹ M. Rehak,² E.P. Rohrer,² J. Royet,⁶ W. Sampson,² P. Sanger,¹ R. Scanlan,⁶ R. Schermer,¹ R. Shutt,² R. Stiening,¹ J. Strait,³ C. Taylor,⁶ R. Thomas,² P. Thompson,² J.C. Tompkins,¹ J. Turner,¹ M. Wake,^{1,4} P. Wanderer,² E. Willen,² Y. Yu,¹ J. Zbasnik,¹ Y. Zhao,¹ and H. Zheng¹

¹ Superconducting Super Collider Laboratory, Dallas, TX 75237 USA

² Brookhaven National Laboratory, Upton, NY 11973 USA

³ Fermi National Accelerator Laboratory, Batavia, IL 60510 USA

⁴ KEK, National Laboratory for High Energy Physics, Tsukuba, Ibaraki 305 Japan

⁵ Korea Electrotechnology Research Institute, Changwon, Kyongnam 641-120, Korea

⁶ Lawrence Berkeley Laboratory, Berkeley, CA 94720 USA

ABSTRACT

This paper summarizes the mechanical performance of the most recent 5-cm-aperture, 15-m-long SSC dipole magnet prototypes. The magnets were produced at Brookhaven National Laboratory (BNL) and Fermi National Accelerator Laboratory (FNAL) in cooperation with the Superconducting Super Collider Laboratory (SSCL). The BNL magnets rely on a horizontally-split yoke with collared ends, while the FNAL magnets rely on a vertically-split yoke with collet-style end clamps. Magnets of both designs are equipped with strain gauges enabling us to measure the azimuthal pressures exerted by the coils against the collar poles as well as the axial forces transmitted from the coil ends to the end plates. A comparison of the mechanical behaviors of the two magnet designs is presented. We also discuss how the behavior of the 5-cm-aperture magnets compares to that of the 4-cm-aperture prototypes.

INTRODUCTION

In January 1990, the decision was taken to increase the aperture of the SSC superconducting dipole magnets from 4 cm¹ to 5 cm.² A large effort was then undertaken at Brookhaven National Laboratory (BNL) and Fermi National Accelerator Laboratory (FNAL) in order to demonstrate the feasibility of the larger aperture magnets. Since then, seven 5-cm-aperture, 15-m-long dipole magnet prototypes have been produced and cold tested at BNL (magnets DCA207 through DCA213), while twelve more have been produced and cold tested at FNAL (magnets DCA311 through DCA322.) The production of the last FNAL magnet (DCA323) is now completed, and the magnet is awaiting its cold testing.

Seven of the FNAL-design magnets (magnets DCA313 through DCA319) were assembled at FNAL by personnel from General Dynamics (GD), and five of the BNL-design magnets (magnets DCA209 through DCA213) were assembled at BNL by personnel from Westinghouse Electric Corporation (WEC). These magnets were part of a technology transfer program from the National Laboratories to the dipole magnet contractors. Five of these industrially-assembled dipole magnet prototypes are used in a string test currently under way at SSCL.³

*Operated by the Universities Research Association, Inc., for the U.S. Department of Energy under Contract No. DE-AC02-89ER40486.

All the 5-cm-aperture, 15-m-long dipole magnet prototypes were cold-tested following the same generic test plan. The plan calls two testing cycles separated by a warm-up to room temperature. Each testing cycle includes quench tests, mechanical measurements, and magnetic measurements. Reference 4 presents a detailed review of the mechanical and quench performance of the early full-length prototypes (BNL magnets DCA207 through DCA209, and FNAL magnets DCA311 through DCA315). In this paper, we summarize the mechanical behavior during cooldown and energization of all the prototypes cold-tested so far. The quench performance of these magnets is discussed elsewhere.⁵

MAGNET FEATURES

The BNL and FNAL magnets are based on the same magnetic design,⁶ and rely on the same concepts for their mechanical design.⁴ The field is produced by a two-layer coil, which is mechanically restrained by means of laminated stainless steel collars. The collars are designed to provide a large azimuthal pre-compression to the coil in order to compensate the effects of the azimuthal component of the Lorentz force. The collared-coil assembly is encased in a laminated iron yoke, around which a stainless steel outer shell is welded. Yoke and shell are designed to tightly clamp the collared-coil assembly in order to stiffen the support against the radial and axial components of the Lorentz force. The main difference between the BNL and FNAL mechanical designs is in the way this clamping is realized. In the BNL design, the yoke is split horizontally and the clamping results from a positive collar-yoke interference along the vertical diameter. In the FNAL design, the yoke is split vertically, and the collar-yoke interference is along the horizontal diameter.

Other specific features of the BNL design include internal splices between the inner and outer conductors, located at the radius of the outer coil, and the fact that the coil ends are supported radially by collars similar to that of the magnet body. In the FNAL design, the splices are made at a radius larger than that of the outer coil, and the coil ends are supported by a four-piece G10 collet that is compressed radially by a tapered, aluminium cylinder. In both designs, the coil ends are loaded axially by four screws mounted into a



thick stainless end plate that is welded to the outer shell. Details of the features and construction of these magnets can be found in references 4, and 7 through 9.

For most of the prototypes, the cable insulation consists of a 25- μm -thick layer of Kapton, wrapped with a 50% overlap, completed by a 125- μm -thick layer of epoxy-impregnated fiberglass, wrapped with a 0.5-mm gap. The last two BNL magnets (DCA212 and DCA213), however, use a so-called *all-Kapton* insulation scheme, which consists of two layers of Kapton (30 μm and 34 μm in thickness, respectively), wrapped with a 50% overlap, and with a polyimide adhesive coating on the outer surface of the second layer. Similarly, the inner cable insulation of the last four FNAL magnets (DCA320 through DCA323) consists of two 25- μm -thick layers of Kapton, wrapped with a 50% overlap, while the outer cable insulation consists of a 25- μm -thick layer of kapton, wrapped with a 50% overlap, completed by a 25 μm -thick layer of Kapton, butt-wrapped with no overlap. For both the inner and outer coils of magnets DCA320 and DCA321, B-stage epoxy is coated on the outer surface of the second Kapton layer, while the second Kapton layer of magnets DCA322 and DCA323 is coated with Cryorad on both sides. Discrepancies in coil sizes resulting from the changes in cable insulation are compensated by adjusting the pole shim thickness (BNL magnets), or by installing brass shims next to the copper wedges and at the collar poles (FNAL magnets). The nominal curing temperature is 135 °C, except for magnets DCA212 and DCA213, which use 225 °C.

STRAIN GAUGE INSTRUMENTATION

The BNL and FNAL magnets are instrumented with two types of strain-gauge transducers:¹⁰ 1) beam-type strain-gauge transducers, located at the collar poles and measuring the azimuthal pressures exerted by the coils, and 2) bullet-type strain-gauge transducers, located in the axial loading screws and measuring the force exerted by the coil against the end plates. The FNAL magnets have two strain-gauge collar packs, located respectively at the minimum and and the maximum of the azimuthal coil sizes, while the BNL magnets have only one, located at the minimum. (Each strain-gauge collar pack totals eight transducers.) Both ends of the BNL magnets are instrumented with bullet gauges, while only the non-lead end of the FNAL magnets is instrumented.

EXPECTED BEHAVIOR

During Cooldown

During cooldown, the various parts of the magnet shrink at different rates. In the azimuthal direction, the coil shrinks more than the Nitronic-40 stainless steel collars, resulting in a decrease of the pressure against the collar poles. On the 4-cm-aperture magnets, a clear correlation was established between the amplitude of the cooldown loss and the pressure at room temperature.¹¹ This was interpreted as an effect resulting from the non-linearity of the coil stress-strain curve: the higher the room temperature pre-compression, the stiffer the coil, and, for a given thermal shrinkage differential between the collars and the coil, the faster the rate of loss during cooldown.

In the radial direction, the Nitronic-40 stainless steel collars shrink more than the low carbon steel yoke. This results in a decrease of the collar-yoke interference along the axis where it is provided, while a gap develops or grows along the other axis. Table 1 summarizes the estimated collar-yoke interferences at room and liquid helium (LHe) temperatures for the nineteen prototypes discussed in this paper. For the BNL magnets, the numbers correspond to the interference along the vertical diameter, while, for the FNAL magnets, it corresponds to the horizontal diameter. The room-temperature values are based on actual measurements of the collared-coil assembly diameters, while the LHe-temperature values are deduced from the room-temperature estimates by taking into account the difference in thermal expansion coefficients between the collar and yoke steels. It appears that, for most of the BNL magnets, the collar-yoke interference is much smaller than that of the FNAL magnets.

In the axial direction, the outer stainless steel shell is expected to shrink more than the coil, thus resulting in an increase of the axial loading. In reality, however, the whole structure is tightly clamped radially, and axial motions of the cold mass components are restrained by friction. The end-force change during cooldown is thus somewhat unpredictable.

Table 1. Summary of collar-yoke interferences. (Warm and cold refer to room and LHe temperatures, respectively.)

Magnet	BNL Magnets Interferences (μm)		FNAL Magnets Interferences (μm)		
	Warm	Cold	Warm	Cold	
DCA207	170	35	DCA311	330	195
DCA208	167	32	DCA312	340	205
DCA209	162	27	DCA313	335	200
DCA210	128	-7	DCA314	290	155
DCA211	186	50	DCA315	285	150
DCA212	175	39	DCA316	277	141
DCA213	226	90	DCA317	249	113
			DCA318	173	37
			DCA319	213	78
			DCA320	264	128
			DCA321	277	141
			DCA322	262	128

During Energization

The Lorentz force has three main components which are applied to the coil during energization: 1) an azimuthal component, which tends to compress the two coil layers towards the midplane and to unload the collar poles; 2) a radial component, which tends to bend the collars outwardly, with a maximum deflection at the midplane; and 3) an axial component, which tends to stretch the coil ends. During energization, the pressure against the collar pole is thus expected to decrease as a function of current squared, while the force against the end plate is expected to increase. Furthermore, in the case of the BNL magnets, the cooldown shrinkage differentials result in a gap between the collared-coil assembly and the yoke along the horizontal diameter. During energization, the radial component of the Lorentz force thus

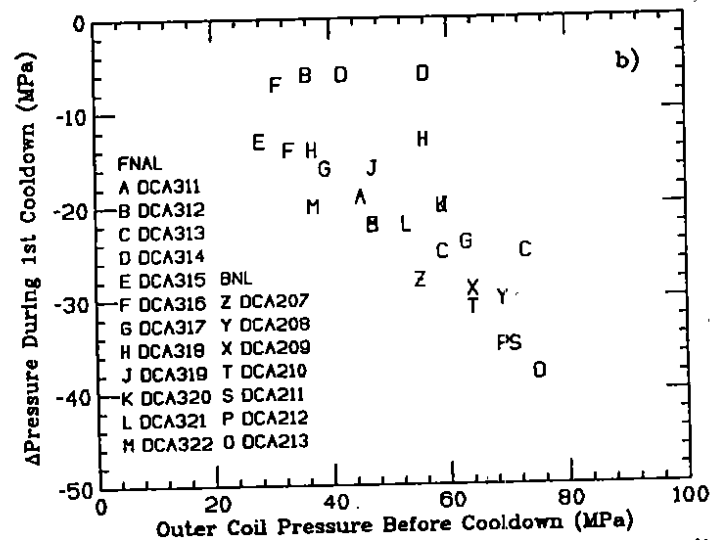
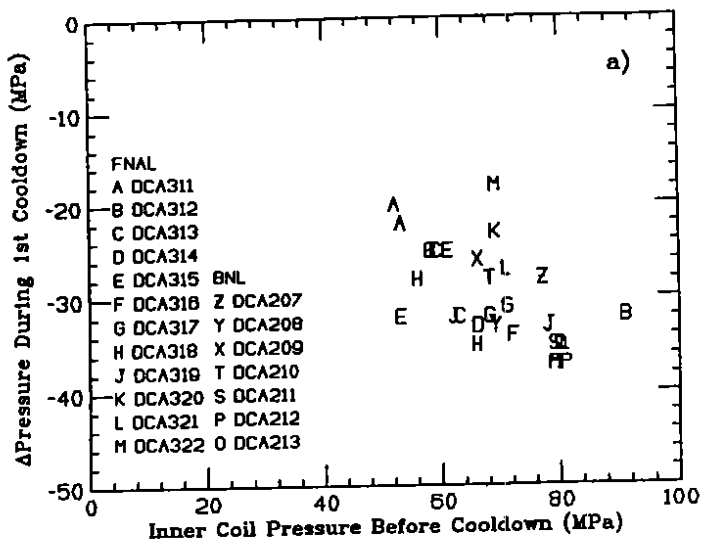


Fig. 1. Coil pressure change during cooldown vs. coil pressure at room temperature: a) inner layer, b) outer layer.

bends the collars and the coil deflects accordingly. This increase of the coil arc length results in a decrease of the coil pressure, thereby enhancing the unloading rate of the collar pole.^{4,11} This unloading rate is also expected to be affected by the non-linearity of the coil stress-strain curve, and thus to depend on the level of pre-compression at zero current.

The axial component of the Lorentz force is estimated to be of the order of 2.1 kN/kA^2 ,¹² and distributes itself as a compressive load against the end plates and an extensive force on the coil body.^{4,11}

COOLDOWN

Coil Pressure

Figure 1 summarizes the change in coil pressure during cooldown as a function of the coil pressure at room temperature for the nineteen magnets discussed in this paper. (For each strain gauge pack of each magnet, the pressures are averaged over the four quadrants of the given coil layer). As expected, the cooldown loss appears to increase quasi-linearly as a function of the room-temperature pressure, and the slope is similar for both inner and outer layers. Between 40 to 50 %

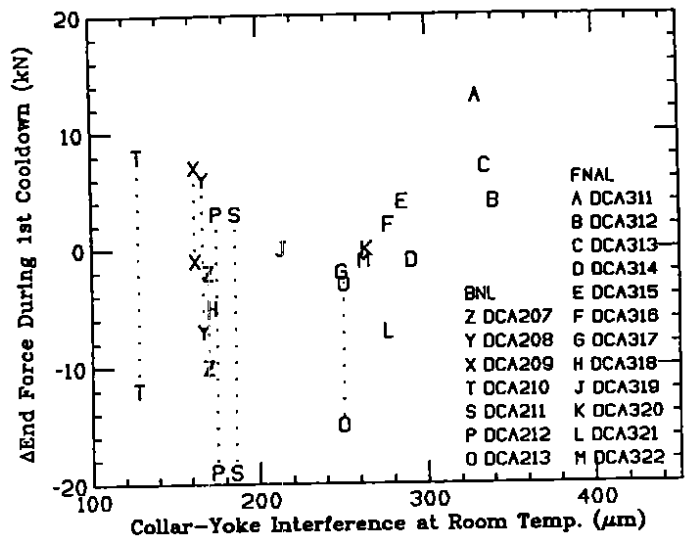


Fig. 2. End-force change during cooldown vs. warm collar-yoke interference. (For the BNL magnets, dotted lines connect the data from the two ends.)

of the room temperature pre-compression is lost during cooldown. Note that the all-Kapton insulation magnets behave similarly to the other magnets.

End Force

One parameter determining the end-force change during cooldown is thought to be the collar-yoke interference at room temperature.¹¹ Figure 2 presents a summary of the end-force change during cooldown as a function of the estimated collar-yoke interference at room temperature. The data from the BNL magnets appear somewhat scattered, and there is a large difference between the lead end and the non-lead end of the magnets. The data from the FNAL magnets, however, appear more reproducible, and lie on a line with a positive slope. One explanation for this more reproducible behavior of the FNAL magnets may be that the larger collar-yoke interference forces collared-coil assembly, yoke, and shell to move more evenly during cooldown. The origin of the positive slope is not yet understood.

ENERGIZATION

Coil Pressure

Figure 3(a) presents a summary of the coil inner-layer pressure as a function of current squared for the BNL magnets, while Fig. 3(b) presents a similar plot for the FNAL magnets. The data displayed in Fig. 3 were taken during strain-gauge runs performed after the quench plateau had been established. For each magnet, the pressures are average over the four quadrants of a selected strain-gauge pack, and only current up-ramp data are displayed. For the BNL magnets, the unloading rates at low currents appear to be much faster than those of the FNAL magnets, while, at higher currents, the traces flatten and become nearly parallel to those of the FNAL magnets. Figures 4(a) and 4(b) present similar plots for the outer-layer pressure. The traces exhibit the same features as those in Fig. 3, except that the unloading rates are much slower. In addition, in Fig.

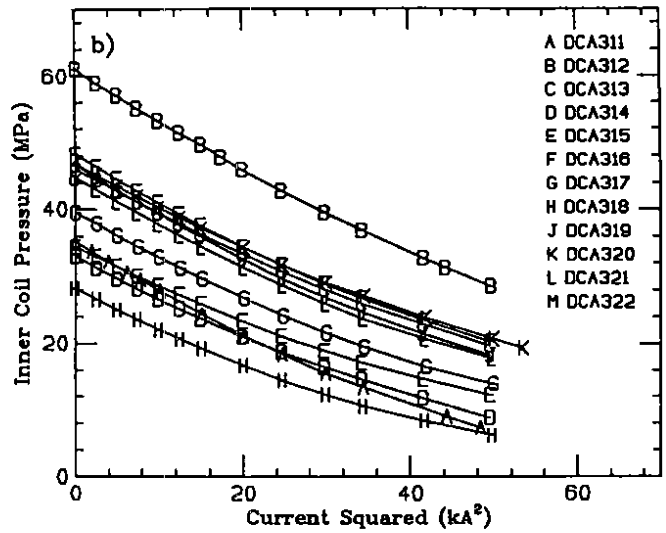
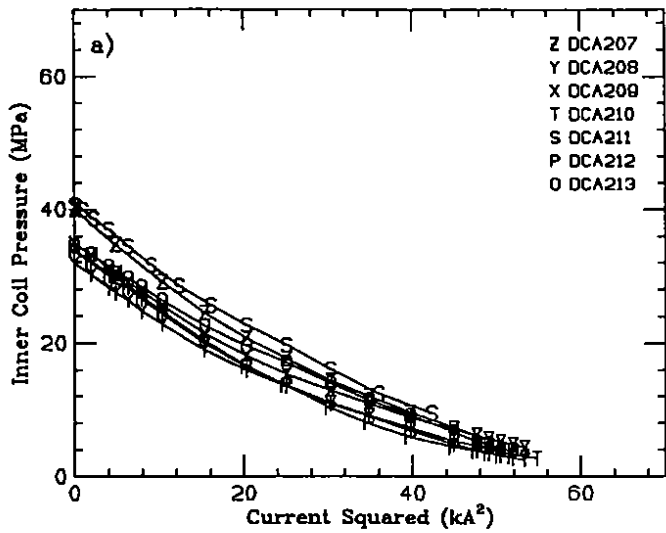


Fig. 3. Coil Inner-layer pressure versus current squared: a) BNL magnets, b) FNAL magnets.

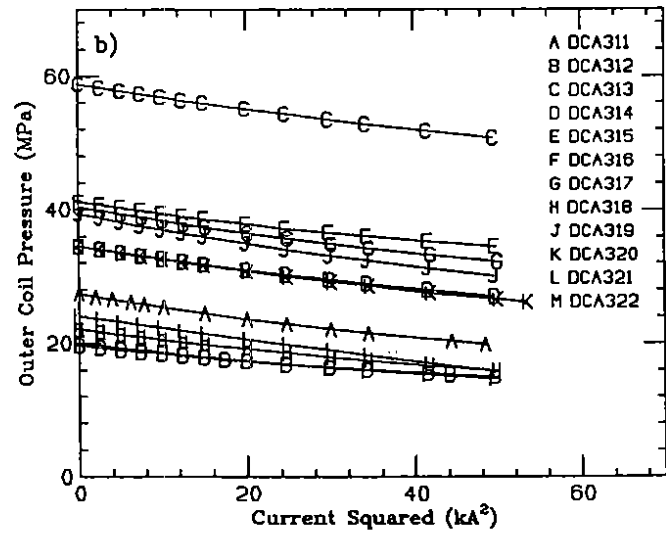
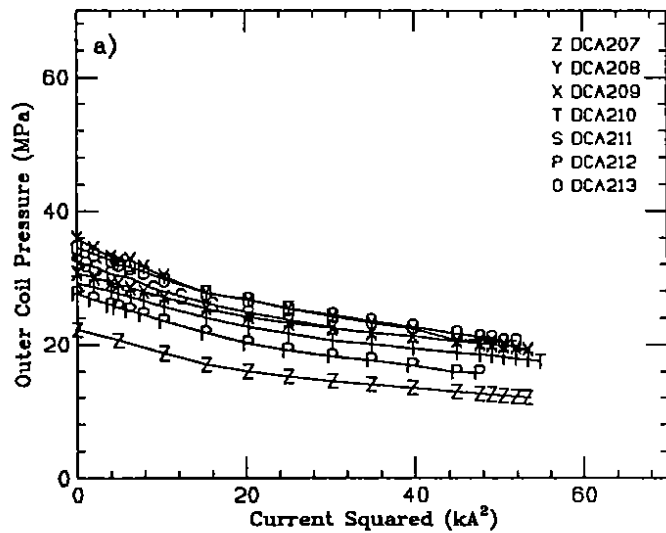


Fig. 4. Coil Outer-layer pressure versus current squared: a) BNL magnets, b) FNAL magnets.

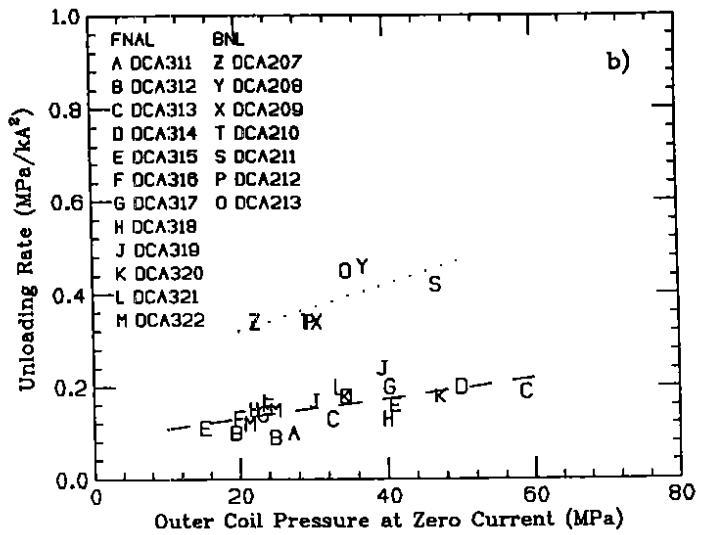
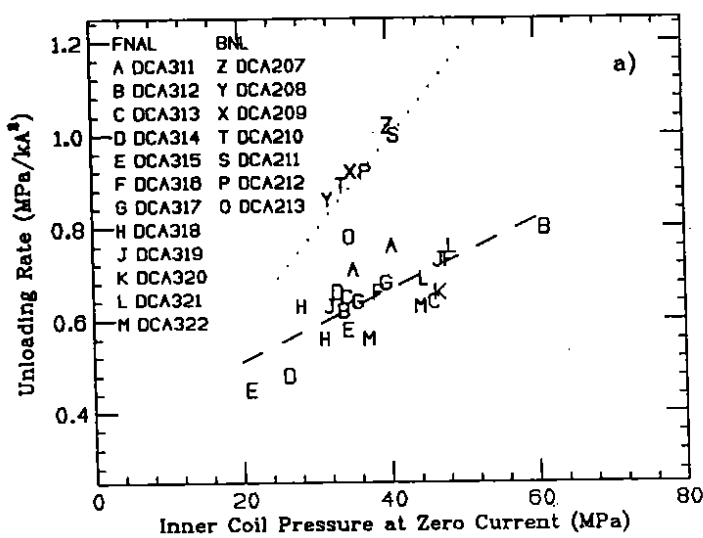


Fig. 5. Coil pressure unloading rate as a function of coil pressure at zero current: a) inner layer, b) outer layer.

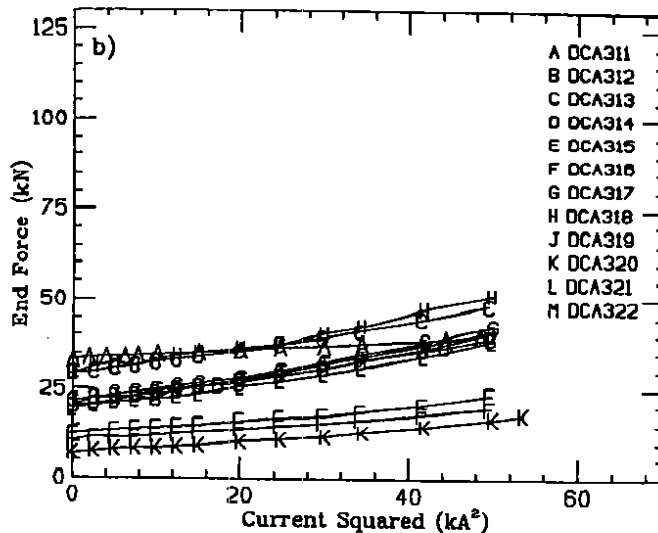
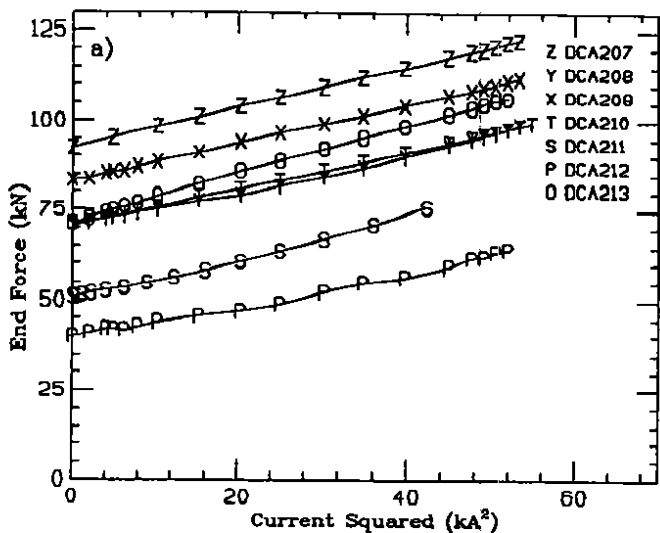


Fig. 6. Total end force versus current squared: a) BNL magnets, b) FNAL magnets.

4(a), the traces of the BNL magnets seem to exhibit a break at a current of about 4000 A. This breaking point is interpreted as the current at which the collared-coil assembly comes into contact with the yoke along the horizontal diameter.^{4,11} For currents larger than the contact current, the BNL magnets behave similarly to the FNAL magnets. Note, once again, that the all-Kapton insulation magnets do not appear to behave differently from the other magnets.

As mentioned earlier, the initial unloading rate of the coil pressure is expected to depend on the coil pressure at zero current. Figure 5(a) presents a summary plot of the initial rate of unloading of the inner-layer pressure as a function of the pressure at zero current. The data clearly separate into two families, which correspond to the two magnet families. Furthermore, each of the families can be fitted by a first order polynomial. Figure 5(b) presents a similar plot for the outer-layer pressure. Similarly to Fig. 5(a); the data separate into two families which can be fitted by a first order polynomial. In both figures, the dotted lines correspond to a linear fit of the BNL data, while the dashed lines correspond to a linear fit of the FNAL data. The dotted lines are always above the dashed lines and have steeper slopes.

Using a simple spring model,¹³ the unloading rate of the coil pressure against collar pole can be predicted to be of the order of 0.55 MPa/kA² for both inner and outer layer. The unloading rates of the FNAL coil inner layers are consistent with this prediction. On the other hand, for the BNL magnets, the radial component of the Lorentz force causes the collars to bend outwardly, resulting in an increase of the arc length of the collar cavity, which enhances the coil pressure unloading rate. This explains why the dotted lines are above the dashed lines. Furthermore, as we also discussed above, the coil stress-strain curve is non-linear: the higher the pressure, the stiffer the coil. This explains why, although the Lorentz load is the same magnet-to-magnet, the four lines have a positive slope. Finally, since for the BNL magnets, the effects of the azimuthal component of the Lorentz force are combined with an increase of the arc length of the collar cavity, the effects of

the non-linearity of the coil stress-strain curve are felt more severely. This explains why the dotted lines have steeper slopes than the dashed lines. The reason why the outer-layer unloading rates are much slower than the inner-layer ones is not clear. A possible explanation is that the radial pressure exerted by the inner layer restricts the unloading of the outer layer. Despite these slower rates, however, the amplitude of the difference between the BNL and FNAL magnets is of the same order of magnitude as that seen for the inner layer. This indicates that both layers of the coil have similar responses to collar deflections, which is consistent with what was observed for the cooldown data in Figs. 1(a) and 1(b).

End Force

Figure 6(a) presents a summary of the end force versus current squared for the non-lead end of the BNL magnets, while Fig. 6(b) presents a similar plot for the FNAL magnets. The data displayed in Fig. 6 were taken during the same strain-gauge run as in Figs. 3 and 4, and correspond to the sum of the four bullet gauges. The end force loading rates of the FNAL magnets appear to be much smaller than that of the BNL magnets. This can be explained by the fact that the FNAL magnets have a larger collar-yoke interference, and that more of the axial component of the Lorentz force can be shared by friction between collared-coil assembly, yoke, and shell. (For the FNAL magnets, only 10 to 15% of the axial component of the Lorentz force is transmitted to the end plates.)

Figure 7 presents a summary plot of the initial loading rate of the end force as a function of the end force at zero current. Once again, the data appear to separate into two families, which correspond to the two magnet families. (One exception is FNAL magnet DCA311, which is known to have had yoke and end parts assembly problems.^{4,14}) The dotted and dashed lines correspond to a linear fit of the BNL and FNAL data, respectively. The dashed line appears to have a steeper slope than that of the dotted line, possibly revealing that the collet-style FNAL ends have a more non-linear compliance than the simpler BNL ends.

CONCLUSION

The mechanical performance of the BNL and FNAL magnets correspond to their somewhat different designs, and no difference in behavior is observed between the various insulation schemes that were tried. A good qualitative understanding of the mechanical characteristic of these magnets was achieved. To carry out a more precise quantitative analysis, a finite element model including non-linear material properties at a level more advanced than is currently available would be required.

REFERENCES

- 1 J.D. Jackson, ed., "Conceptual Design of the Superconducting Super Collider," SSC-SR-1020, March 1986; revised, September 1988.
- 2 J.R. Sanford and D.M. Matthews, eds., "Site-Specific Conceptual Design of the Superconducting Super Collider," SSCL-SR-1056, July 1990.
- 3 A.D. McInturf, J.G. Weisend II, *et al.*, "SSCL Half Cell Operational Test," in these Proceedings.
- 4 A. Devred, T. Bush, *et al.*, "Review of SSC Dipole Magnet Mechanics and Quench Performance," to appear in *Supercollider 4*, J. Nonte, ed., 1992.
- 5 W. Nah, A. Akhmetov, *et al.*, "Quench Performance of 5-cm-Aperture, 15-m-Long SSC Dipole Magnet Prototypes," in these Proceedings.
- 6 R.C. Gupta, S.A. Kahn, and G.H. Morgan, "SSC 50 mm Dipole Cross Section," *Supercollider 3*, J. Nonte, ed., 1991, pp. 587-599.
- 7 J. Strait, K. Coulter, *et al.*, "Experimental Evaluation of the Vertically versus Horizontally Split Yokes for SSC Dipole Magnets," *Supercollider 2*, M. McAshan, ed., 1990, pp. 731-741.
- 8 M. Anerella, J. Cottingham, *et al.*, "Construction and Test Results from 15-m-Long, 50-mm-Aperture SSC Dipole," to appear in *Supercollider 4*, J. Nonte, ed., 1992.
- 9 M.J. Blessing, D.E. Hoffman, *et al.*, "Construction Experience with Fermilab-Built Full-Length 50-mm SSC Dipole," to appear in *Supercollider 4*, J. Nonte, ed., 1992.
- 10 C.L. Goodzeit, M.D. Anerella, *et al.*, "Measurement of Internal Forces in Superconducting Accelerator Magnets with Strain Gauges Transducers," *IEEE Trans. Magn.*, 25(2), 1989, pp. 1463-1468.
- 11 A. Devred, T. Bush, *et al.*, "About the Mechanics of SSC Dipole Magnet Prototypes," AIP Conference Proceedings 249(2), 1992, pp. 1310-1374.
- 12 D. Orrel, private communication.
- 13 P. Schmüser, "Superconducting Magnets for Particle Accelerators," AIP Conference Proceedings 249(2), 1992, pp. 1099-1158.
- 14 M. Wake, M. Bleadon, *et al.*, "Mechanical Behavior of Fermilab/General Dynamics Built 15m SSC Dipoles," to appear in *Supercollider 4*, J. Nonte, ed., 1992.

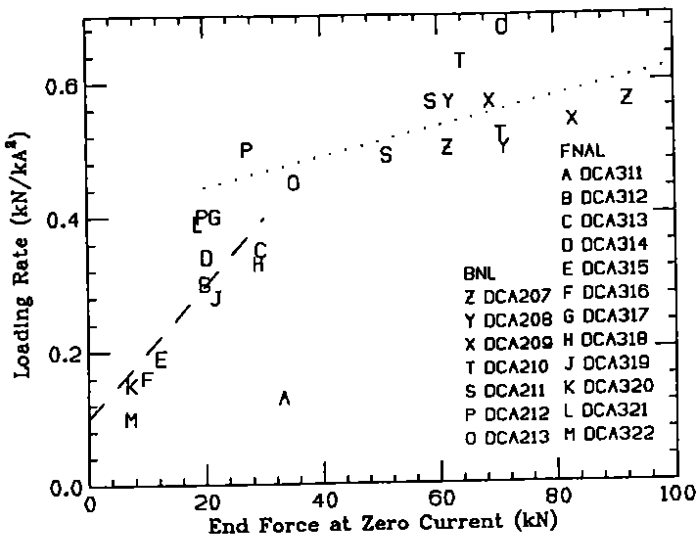


Fig. 7. End force loading rate versus end force at zero current.

As described in previous papers,^{4,11} the BNL magnets exhibit a tendency to built-up end force in the course of their energization cycles. Table 2 presents a summary of end-force measurements after the first cooldown and before the first warm-up of the nineteen prototypes discussed in this paper. The end forces of the BNL magnets all appear to increase significantly during cold-testing, while that of the FNAL magnets remain fairly constant. This end-force build-up, which mainly occurs at the time of the first excitations and quenches, is attributed to stick-slip motions of the collared-coil assembly within the yoke.

Table 2. Summary of end-force change during cold testing. (For the BNL magnets, the letters LE and NL refer to the Lead End and the Non-Lead End, respectively.)

Magnet	BNL Magnets			FNAL Magnets			
	Beg.	End	δ	Magnet	Beg.	End	δ
DCA207LE	54	62	+8	DCA311	33	33	0
DCA207NL	66	90	+24	DCA312	18	20	+2
DCA208LE	51	59	+8	DCA313	29	29	0
DCA208NL	47	68	+11	DCA314	17	20	+3
DCA209LE	51	73	+22	DCA315	12	12	0
DCA209NL	27	88	+61	DCA316	9	11	+2
DCA210LE	33	65	+32	DCA317	20	32	+12
DCA210NL	58	72	+14	DCA318	26	n/a	n/a
DCA211LE	56	69	+13	DCA319	17	22	+5
DCA211NL	46	67	+21	DCA320	5	7	+2
DCA212LE	20	n/a	n/a	DCA321	16	19	+3
DCA212NL	5	n/a	n/a	DCA322	5	7	+2
DCA213LE	27	35	+13				
DCA213NL	25	70	+45				